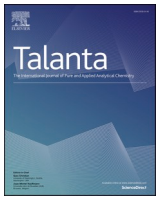
Talanta 291 (2025) 127852



Contents lists available at ScienceDirect

Talanta

journal homepage: www.elsevier.com/locate/talanta



A CRISPR/Cas13a system based on a dumbbell-shaped hairpin combined with DNA-PAINT to establish the DCP-platform for highly sensitive detection of Hantaan virus RNA

Jiamei Zhong [a], Ziyue Xu [a], Jiawei Peng [a], Liwen Guan [a], Jianxiong Li [b], Zhuoxun Zhou [a], Yu Zhang [a], Jie Zhang [a], Shiwen Liu [b,*], Yifei Yang [a,**], Xian Hao [a,***]

[a] School of Public Health &Jiangxi Provincial Key Laboratory of Disease Prevention and Public Health, Jiangxi Medical College, Nanchang University, Nanchang, Jiangxi, 330031, PR China

[b] Laboratory of Viral Infectious Disease, The Key Laboratory of Important and Emerging Viral Infectious Diseases of Jiangxi Health Commission, Jiangxi Provincial Center for Disease Control and Prevention, Nanchang, Jiangxi, 330029, PR China

ARTICLE INFO

Keywords:
RNA detection
CRISPR/Cas13a
Single-molecule fluorescence imaging
DNA-PAINT
Biomarker

ABSTRACT

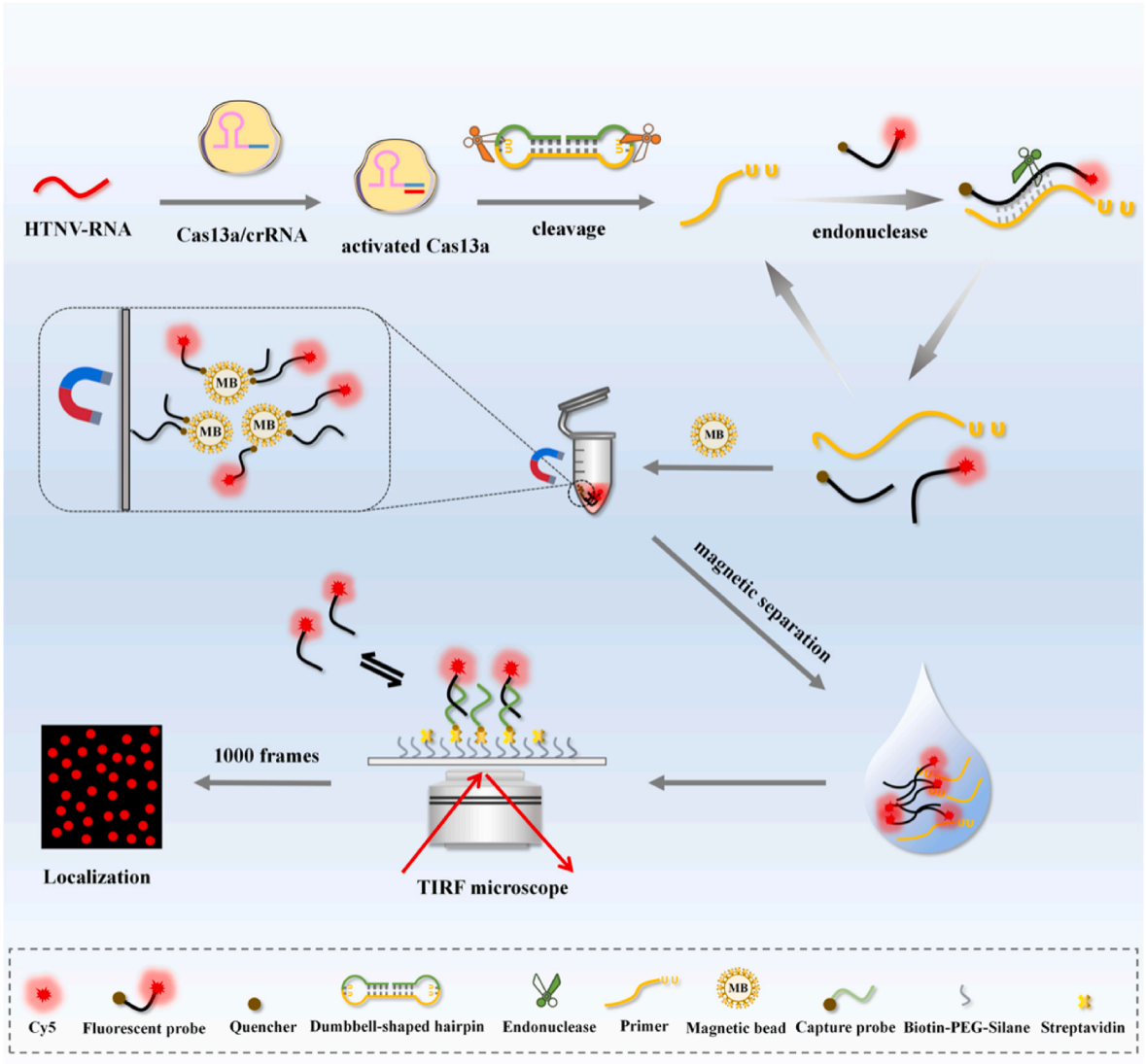
Rapid and sensitive detection of specific RNA sequences is crucial for clinical diagnosis, surveillance, and biotechnology applications. Currently, reverse transcription-quantitative polymerase chain reaction (RT-qPCR) is the gold standard for RNA detection; however, it is associated with long processing time, complex procedures, and a high false-positive rate. To address these challenges, we developed a novel sensing platform based on CRISPR/Cas13a that incorporates a dumbbell-shaped hairpin and DNA-PAINT for rapid, highly specific, and sensitive RNA analysis. By leveraging the CRISPR/Cas13a system, this platform enables the cleavage of dumbbell-shaped hairpins, which subsequently allows the cleaved primers to initiate cyclic amplification of fluorescent signals. These signals are further enhanced by the binding and dissociation phenomena inherent to DNA-PAINT technology, ultimately achieving remarkable triple signal amplification. Additionally, the system effectively discriminates Hantaan virus RNA from Seoul virus in real samples. Importantly, the platform can be easily adapted for the detection of other RNAs by simply reconfiguring the hybridization region of crRNA. In conclusion, this platform represents a "five-in-one" RNA detection approach that integrates reliability, versatility, robustness, high specificity, and superior quantitative capabilities. It provides novel insights for direct RNA detection based on CRISPR/Cas13a and demonstrates significant potential for advancement in viral diagnostics.

1. Introduction

Ribonucleic acid (RNA) serves as a carrier of genetic information in the cells of living organisms, as well as certain viruses and viroids. Abnormalities of RNA content or expression can lead to a variety of diseases [1–3], underscoring the importance of RNA detection for the prevention and treatment of early diseases [4,5]. Currently, RT-qPCR is regarded as the gold standard for nucleic acid detection [6,7]. However, it has several limitations, including lengthy processing times and complex procedures. To overcome these challenges, researchers have developed innovative methods for RNA detection. In recent years, the clustered regularly interspaced short palindromic repeats (CRISPR) and CRISPR-associated proteins (CRISPR-Cas) adaptive immune system has emerged as a prominent tool in gene editing. This system encompasses programmable nucleic acid endonuclease technology, enabling precise and efficient targeting of RNA sequences. In 2017, Zhang et al. [8]. harnessed the ancillary effects of CRISPR-Cas in combination with isothermal amplification techniques—such as recombinase polymerase amplification (RPA) [9], loop-mediated isothermal amplification (LAMP) [10,11], and rolling circle amplification [12]—to establish CRISPR-based diagnostic methods. This advancement has significantly propelled the application of CRISPR-Cas technology in nucleic acid detection. Nonetheless, these methodologies often require multiple enzymes and are susceptible to false positives. To mitigate these issues,

* Corresponding author.
** Corresponding author.
*** Corresponding author.
E-mail addresses: liushiwen985@126.com (S. Liu), yangyifei@ncu.edu.cn (Y. Yang), xian.hao@ncu.edu.cn (X. Hao).

https://doi.org/10.1016/j.talanta.2025.127852
Received 14 January 2025; Received in revised form 24 February 2025; Accepted 26 February 2025
Available online 6 March 2025
0039-9140/© 2025 Elsevier B.V. All rights are reserved, including those for text and data mining, AI training, and similar technologies.



Scheme 1. The CRISPR/Cas13a system is based on a dumbbell-shaped hairpin combined with DNA-PAINT to structure the DCP-platform for highly sensitive detection of Hantavirus RNA.

researchers have explored the integration of CRISPR-Cas with alternative non-amplification methods, including catalytic hairpin assembly (CHA) [13,14], microfluidic chips [15], colorimetric assays [16,17], electrochemistry [18], electrochemiluminescence [19], and nanomaterials [20–22]. Although the sensitivity of RNA detection has significantly improved and false positive rates have decreased, these techniques can involve complex nanomaterial synthesis, intricate chip design processes, prolonged detection times, and inconsistent results. Therefore, there is an urgent need for a novel RNA detection method that is sensitive, rapid, accurate, and straightforward.

Over the past three decades, substantial advancements have been achieved in the fields of single-molecule chemistry [23], molecular dynamics [24], fluorescence correlation spectroscopy (FCS) [25], and other single-molecule fluorescence techniques. These developments have enhanced the application of these techniques in highly sensitive biosensors [26], facilitating the monitoring of dynamic behaviors and interactions of individual biological molecules, thereby illuminating complex biological processes. This progress holds considerable promise for disease prediction and progression analysis. Moreover, single-molecule fluorescence imaging requires minimal sample consumption while offering rapid analytical speeds, making it particularly advantageous for swiftly detecting and quantifying low-abundance biomarkers in complex environments [27]. However, conventional single-molecule fluorescence detection methods face limitations due to a finite number of detectable signals, which restricts their sensitivity [28]. In contrast, DNA point accumulation in nanoscale topology (DNA--PAINT) [29,30] has demonstrated remarkable capabilities, including infinite spectral multiplexing and ultra-high (sub-5-nm) spatial resolution. This methodology relies on the transient binding and dissociation of dye-labeled short DNA oligonucleotides (imaging strands) with their complementary target-binding strands to produce a series of random flashes necessary for super-resolution imaging [31–34]. By utilizing the counts of blinking events as an output signal, this technique allows for ultra-sensitive quantification of target molecules without necessitating enzyme amplification, making it an ideal approach for quantitative biological analysis [35,36]. However, for early viral detection, the limit of detection (LOD) provided by a single DNA-PAINT method is still insufficient.

Therefore, we integrated the CRISPR/Cas13a system, the dumbbell-shaped hairpin, and DNA-PAINT to construct a highly sensitive and highly specific biosensing platform (DCP-platform), enabling the straightforward detection of Hantaan virus RNA (HTNV-RNA) at the single-molecule level. Hantaan virus (HTNV), a zoonotic virus in the *Hantaviridae* family that causes severe hemorrhagic fever with renal

syndrome in humans with fatality rate of 15 % [37]. It is a significant global health concern, and currently, no effective vaccines or treatments are available [38]. In our system, CRISPR/Cas13a is specifically activated by the HTNV-RNA, allowing it to cleave the dumbbell-shaped hairpin and release the primers, thus initiating the first step of amplification. Then, the released primers hybridize with the fluorescent probe to form a double-stranded complex, activating the nucleic acid endonuclease to cleave the fluorescent probe. The freed primers can then bind to additional probes, facilitating a cyclical reaction that results in a significant signal amplification—representing the second step of probe signal enhancement. Following amplification, unbound fluorescent probes are removed by magnetic separation, and the supernatant is used for single-molecule imaging. The fragmented probes interact with capture probes (CPs) immobilized on the coverslip surface, establishing a dynamic equilibrium process of "binding-unbinding" via the TIRF microscope. Each event generates a fluorescence localization signal, and by continuously collecting and analyzing these dynamic occurrences and quantitatively assessing the correlation between the localization frequency and the target concentration, we achieve the third step of single-molecule signal amplification, enabling detection limits as low as attomolar (aM) concentrations.

2. Experimental Section

2.1. Hairpin annealing

To prepare a 10 μL solution of 1 μM dumbbell-shaped hairpin (H1, H2, H3, H4), 1 μL of each 10 μM hairpin was mixed with 2 μL of 5 × Annealing Buffer for DNA Oligos and 7 μL of DEPC-treated water. The mixture was then heated at 95 °C for 5 min to anneal the hairpins, followed by a gradual cooling to room temperature over 40 min. Finally, the annealed hairpin was stored at 4 °C for future use.

2.2. Construction of the DCP-platform

Initially, the Cas13a/crRNA complex was prepared by combining 50 nM LwaCas13a, 25 nM crRNA, 1 × rCutSmart™ buffer, and H2O, followed by incubation at 37 °C. Subsequently, the target nucleic acid was introduced alongside 400 nM hairpin H1, 1 μM fluorescent probe T1, 5 U Nb.BbVCI, and 1 × Annealing Buffer for DNA Oligos, and the mixture was incubated at 35 °C for 30 min. Thereafter, 20 μL of streptavidin-coated magnetic beads were added to each reaction mixture and vortexed for 30 min to facilitate the binding of biotin-labeled fluorescent probe fragments, particularly the intact fluorescent probe, thereby minimizing background signal interference. Following magnetic separation, the supernatant was subjected to fluorescence excitation using a 655–750 nm laser, and fluorescence signals were collected using a fluorescence spectrophotometer at an excitation wavelength of 640 nm. Finally, the supernatant was combined with imaging buffer and applied onto a modified coverslip, after which DNA-PAINT imaging was performed using a TIRF microscope.

The imaging buffer, composed of 100 mM Tris-HCl, 20 mM NaCl, a mixture of 25 mM catalase and glucose oxidase, 10 % glucose solution, 2 mM Trolox (pH 8.0), was used to dilute the supernatant 100-fold. Subsequently, 10 μL of the diluted sample was directly deposited onto the coated coverslip for DNA-PAINT imaging using a TIRF microscope. The Cy5 dye was excited by a 640 nm laser, and emitted photons were collected using a 60 × oil-immersion objective lens (NA 1.45, Olympus) mounted on an Olympus IX73 microscope system. Imaging was performed using a sCMOS camera (Dhyana 95, Tucsen, China). For each sample, five randomly selected regions (with a representative imaging range of 22.09 μm × 22.09 μm in this study) were continuously imaged for 1000 frames at an exposure time of 100 ms. The acquired images were subsequently analyzed, fitted, and quantified using ImageJ software with the Thunderstorm plugin.

2.3. RNA detection in 10 % fetal bovine serum

The serum samples were pretreated according to the previously reported method [39]. Initially, 10 % fetal bovine serum was incubated at 65 °C in a water bath for 30 min to ensure the inactivation of nucleases. Subsequently, 10 μL of the treated serum was introduced into the CRISPR/Cas13a reaction system. Finally, the samples were analyzed by spiking varying concentrations of RNA using the standard addition method.

3. Results and discussion

3.1. The working principle of the DCP-platform

Scheme 1 showed the specific working principle of the sensing platform we have built. First, we designed a dumbbell-shaped hairpin H1 and a fluorescent probe. Considering that the *trans*-cleavage activity of LwaCas13a preferentially cleaves the nucleotide-phosphate diester bond adjacent to uridine residues, the two rings of the dumbbell-shaped hairpin respectively incorporated two uridine nucleotides (rUrU), while the stem contained a primer sequence (14 nucleotides) capable of binding to the fluorescent probe (FP). The fluorescent probe included a specific recognition and cleavage sequence of nucleic acid endonucleases(GC TGAGG), modified with biotin at its 5′ end and a Cy5 fluorophore at its 3′ end. Upon addition of target HTNV-RNA, HTNV-RNA assembled with the spacer region of crRNA through base-pair complementarity to activate the Cas13a protein. Then activated Cas13a engaged in collateral cleavage of nearby H1, releasing abundant primer H1′, which facilitated signal amplification in the first step of the CRISPR/Cas13a system. Next, the released H1′ hybridized with fluorescent probe T1 to form a double-stranded DNA. The newly formed double-stranded DNA was specifically recognized and cleaved by endonuclease in the precise site 5′···C C T C A G C···3′ 3′··· G G A G T C G···5′, resulting in the cleavage of the probes. Then, H1′ could bind to additional probes, producing a significant amount of ssDNA products that facilitated the second-step amplification. Subsequently, we introduced streptavidin-coated magnetic beads into the reaction system to selectively remove the intact fluorescent probe and biotin-modified fluorescent probe fragments through the strong affinity between streptavidin and biotin, and the fluorescent probe fragments containing fluorophores (5' end) were retained in the supernatant. Following this, the supernatant was mixed with the imaging buffer for single-molecule imaging. To facilitate single-molecule imaging, we passivated and biotinylated the coverslip surfaces using Biotin-PEG-Silane and immobilized biotinylated CPs on them by leveraging the high affinity between streptavidin and biotin. Given that CPs and Cy5-modified fluorescent probe fragments possess short complementary base pairs (~8 bp), a dynamic equilibrium of "binding-unbinding" can be established via a TIRF microscope for DNA-PAINT imaging. We documented the binding process of FPs and CPs for fluorescence localization. Considering this process was inherently random and reproducible, the number of localizations significantly surpassed that observed in traditional single-molecule imaging techniques. By continuously acquiring 1000 frames of fluorescence images, we could substantially enhance the signal to accomplish the third stage of single-molecule signal amplification. Consequently, we could achieve a notable reduction in detection limits by employing this 'triple signal amplification method' to identify lower-abundance nucleic acid biomarkers.

3.2. Feasibility of the DCP-platform for RNA detection

To assess the feasibility of the constructed platform, we conducted a series of experiments using the HTNV-RNA sequence as a model target. First, the *trans*-cleavage and endonuclease activities of CRISPR/Cas13a were validated through non-denaturing polyacrylamide gel electrophoresis (PAGE). Since the T1 sequence is too short to effectively

Table 1
The results of Spiked recovery experiments in 10 % FBS (n = 3).

	Sample	Added	Detected	Recovery (%)	RSD (%)
10 % FBS	1	1 pM	1.11 pM	111.43 %	1.72
	2	100 fM	93.33 fM	93.33 %	2.84
	3	10 fM	10.72 fM	107.16 %	2.74

visualize on a gel, we designed an extended chain, T2 (Table 1), to replace the gel run while maintaining the specificity of the sequence. In the absence of the target, the *trans*-cleavage activity of CRISPR/Cas13a was silenced, resulting in unchanged band positions for H1 and T2 (Fig. 1A, lanes 4, 5, and 9). Upon the addition of the target, the H1 band disappeared, and a new band emerged (Fig. 1A, lane 6), indicating successful activation and cleavage of H1 by CRISPR/Cas13a. Following the introduction of T2, the cleaved H1′ formed a double-stranded complex with T2, resulting in the appearance of a new band (Fig. 1A, lane 7). This band disappeared upon the addition of endonuclease, indicating that the formed double-stranded complex effectively activated the nuclease activity, leading to the cleavage of the fluorescent T2 (Fig. 1A, lane 8). Then, we performed fluorescence emission spectroscopy on the supernatant following magnetic separation. The result shown in Fig. 1B and Fig. S1 indicated that a distinct fluorescence signal was generated only in the presence of the target. Furthermore, compared with the sample without endonuclease addition, the fluorescence signal significantly increased after endonuclease was added. This finding suggested that CRISPR/Cas13a could accurately identify the target and cleave the H1 by its activated *trans*-cleavage. The resultant H1' bound to the T2, forming a double-stranded complex that activated endonuclease activity to cleave T2.

Subsequently, the supernatant was utilized for DNA-PAINT imaging. To minimize the background signal interference, the supernatant solution was diluted 100-fold prior to deposition onto pre-modified coverslips for single-molecule imaging. As illustrated in Fig. 1C–D and Movie S1, a substantial number of fluorescence localization signals were observed in the presence of target RNA, whereas only minimal non-specific fluorescence localization signals were detected in its absence. The fluorescence localization count in the target group was 9.42-fold higher than that in the blank group. These findings further validate the feasibility of the proposed platform for RNA detection.

3.3. Optimization of the experimental conditions

To achieve optimal analytical performance, we systematically optimized the experimental conditions. First, the CRISPR-crRNA incubation parameters, including crRNA and Cas13a concentrations, incubation time, and temperature, were refined. Subsequently, the conditions for the hairpin-and-probe cleavage reaction were optimized, encompassing the concentration and sequence of H1 and T1, reaction temperature, duration, buffer composition, and magnetic bead attachment methodology. Additionally, the quantity of magnetic beads and the concentration of CPs for single-molecule fluorescence imaging were optimized. Detailed optimization results are presented in Fig. 2, Figs. S2–S7, and Movie S2. Ultimately, the following optimal experimental conditions were established: (a) For CRISR-crRNA incubation: crRNA concentration of 25 nM, Cas13a concentration of 50 nM, incubation time of 15 min, and incubation temperature of 37 °C; (b) For catalyzing hairpin and probe cleavage: H1 concentration of 400 nM, T1 concentration of 1 μM, reaction temperature of 35 °C, reaction time of 30 min, and using a single nucleic acid endonuclease buffer; (c) For magnetic bead use: 20 μL of magnetic beads were utilized and the reaction was first cleaved and then magnetically separated; (d) For single-molecule fluorescence imaging: the concentration of CP was set at 100 nM.

3.4. Performance analysis of RNA detection

Under the optimized experimental conditions, the detection sensitivity of the CRISPR/Cas13a method was first evaluated using a series of the target RNA concentrations (1 nM, 100 pM, 10 pM, 1 pM, 100 fM, 10 fM, 1 fM, 100 aM, 10 aM). The fluorescence spectra (Fig. 3A) demonstrated a gradual decrease in fluorescence intensity as the target concentration decreased. Notably, a strong linear correlation was observed between the logarithm of the target concentration and the fluorescence intensity within the range of 1 fM to 10 pM (Fig. S8). Subsequently, the sensitivity of the DCP-platform was further investigated using single-molecule fluorescence detection. Fluorescence signals were directly observed in the images captured at various target concentrations when the supernatant was used for single-molecule imaging (Fig. 3B). The fluorescence localizations were quantified, and the processed data (Fig. 3C–D and Movie S3) revealed a concentration-dependent reduction in fluorescence signal counts as the target concentration decreased. Within the range of 1 pM–100 aM, a strong linear relationship was

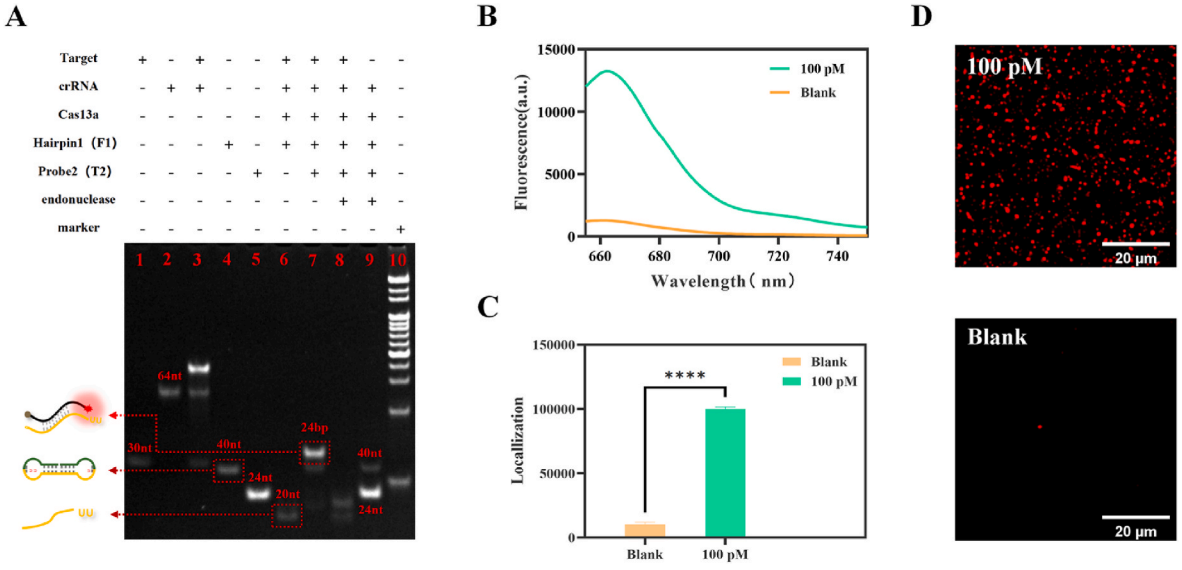


Fig. 1. Feasibility investigation of the DCP-platform for detecting RNA. (A) The non-denaturing polyacrylamide gel electrophoresis experiment. (B) The measurement of Cy5 fluorescence emission spectra. (C) The measurement of Cy5 fluorescence spot counting. The error bars represent the standard deviation of the three experiments. ****$P < 0.0001$, student's *t*-test. (D) The single-molecule fluorescence imaging of Cy5.

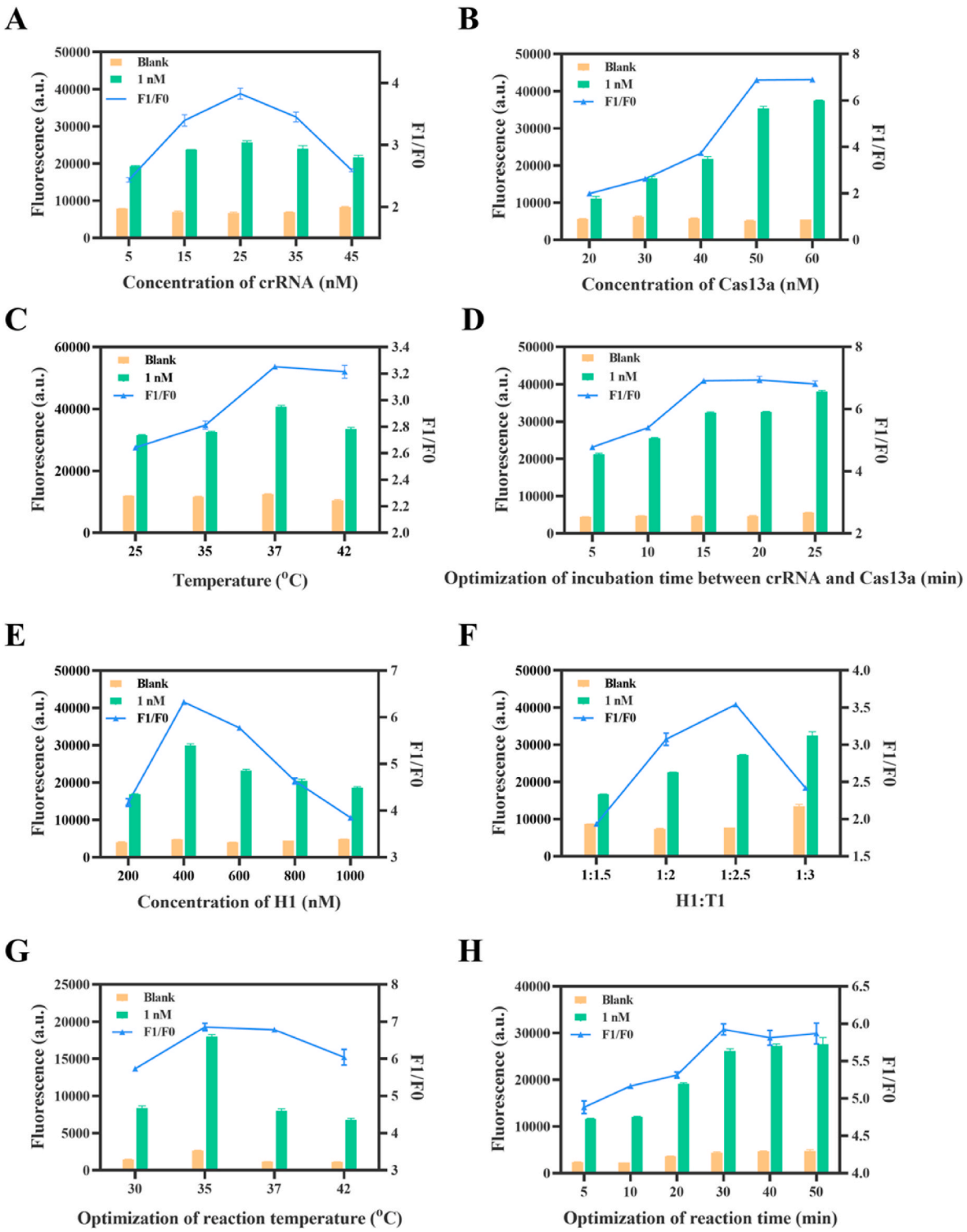


Fig. 2. Optimization of the experimental conditions. (A) Optimization of the concentration of the designed crRNA. (B) Optimization of the concentration of CRISPR/Cas13a. (C) Optimization of the incubation temperature of Cas13a-crRNA. (D) Optimization of the incubation time of Cas13a-crRNA. (E) Optimization of the concentration of H1. (F) Optimization of the ratio of H1 to T1. (G) Optimization of the reaction temperature of the Cas13a-dumbbell hairpin system. (H) Optimization of the reaction time of the Cas13a-dumbbell hairpin system.

observed between the logarithm of the target concentration and the fluorescence signal counts. The linear equation was established as: Y = 22545 X – 38803, with the determination coefficient (R^2) of 0.9505 (where Y represents the localizations counts and X denotes $lgC_{HTNV\text{-}RNA}$). The limit of detection (LOD) was calculated to be 74.13 aM, which is significantly lower than the 5.55 fM obtained from fluorescence measurements. This result demonstrate that the integrating the CRISPR/Cas13a system with the single-molecule fluorescence imaging significantly enhances RNA detection capability. Unlike traditional PCR and other conventional methods [40,41], this biosensor eliminates the need for amplification of the target RNA, thereby mitigating biases and errors associated with amplification processes and improving detection

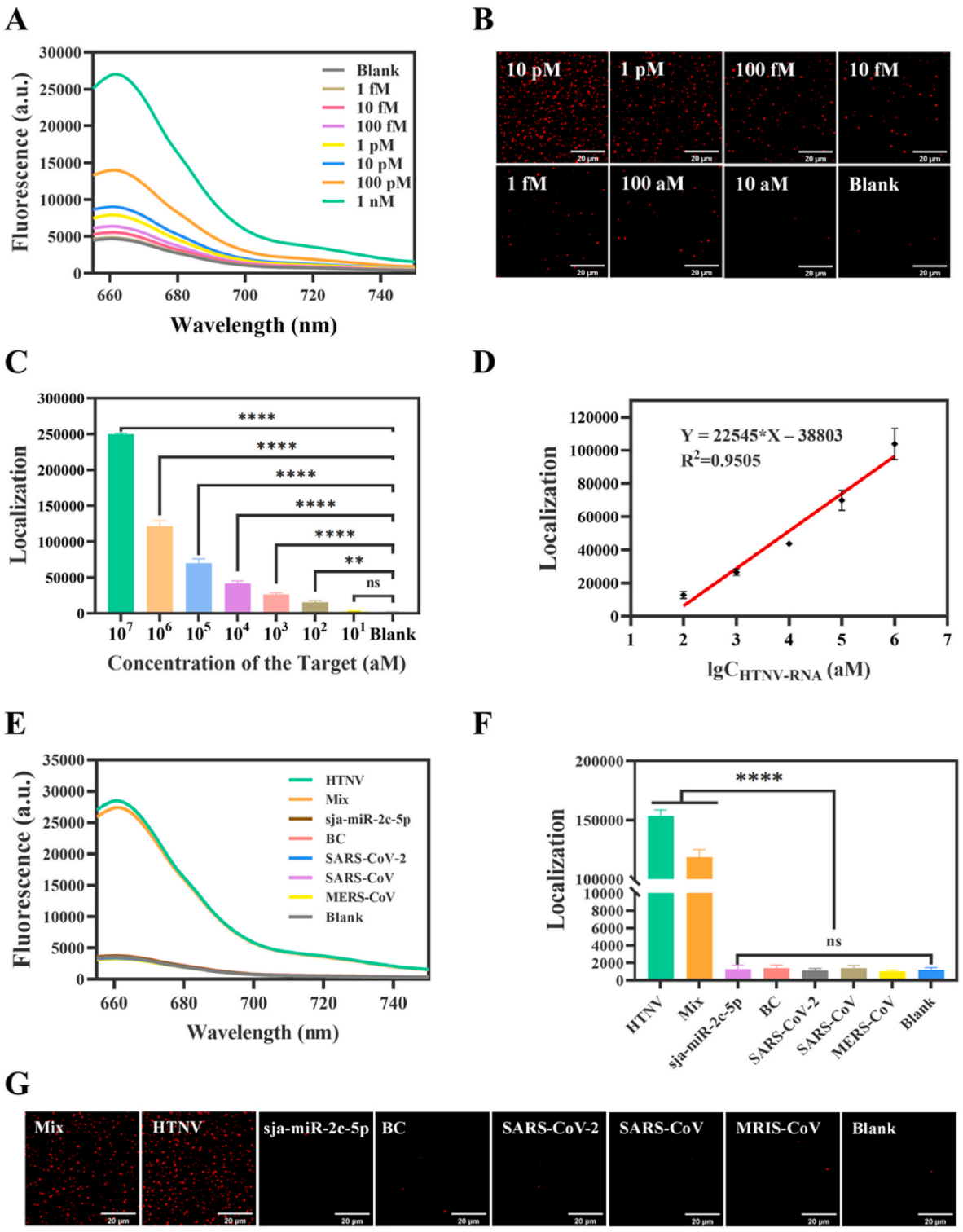


Fig. 3. The sensitivity and specificity of the platform for RNA detection. (A) Measuring the fluorescence emission spectra of the target molecules at different concentrations (1 nM, 100 pM, 10 pM, 1 pM, 100 fM, 10 fM, 1 fM) in the detection system. The blank group served as the negative control group without the target. (B) The single-molecule fluorescence imaging of the supernatant after magnetic separation of the target molecules at different concentrations (10 pM, 1 pM, 100 fM, 10 fM, 1 fM, 100 aM, 10 aM). (C) The single-molecule fluorescence localization analysis of the target at different concentrations (10 pM, 1 pM, 100 fM, 10 fM, 1 fM, 100 aM, 10 aM). Error bars show the standard deviation of three experiments. $^{*}P < 0.05$, $^{**}P < 0.01$, $^{***}P < 0.001$, $^{****}P < 0.0001$, student's *t*-test. (D) The linear relationship between fluorescence localization and logarithm of RNA concentration, ranging from 1 pM to 100 aM. Error bars show the standard deviation of three experiments. (E) The fluorescence emission spectra in the presence of different RNAs (sja-miR-2c-5p, SARS-CoV-2, BC, SARS-CoV, MERS-CoV, HTNV-RNA, and Mix) with blank group as negative control without target and mixed group as detection with 6 RNAs (sja-miR-2c-5p, SARS-CoV-2, BC, SARS-CoV, MERS-CoV, HTNV-RNA) mixed into the reaction solution. (F) The fluorescence localization counts of the target at different concentrations (sja-miR-2c-5p, miR-21, miR-221-3p, piRNA-54265, HTNV-RNA, and Mix) and performing magnetic bead-based purification. $^{*}P < 0.05$, $^{**}P < 0.01$, $^{***}P < 0.001$, $^{****}P < 0.0001$, student's *t*-test. (G) The single-molecule fluorescence imaging of the supernatant of the target at different concentrations (sja-miR-2c-5p, BC, SARS-CoV-2, SARS-CoV, MERS-CoV, HTNV-RNA, and Mix) and performing magnetic bead-based purification.

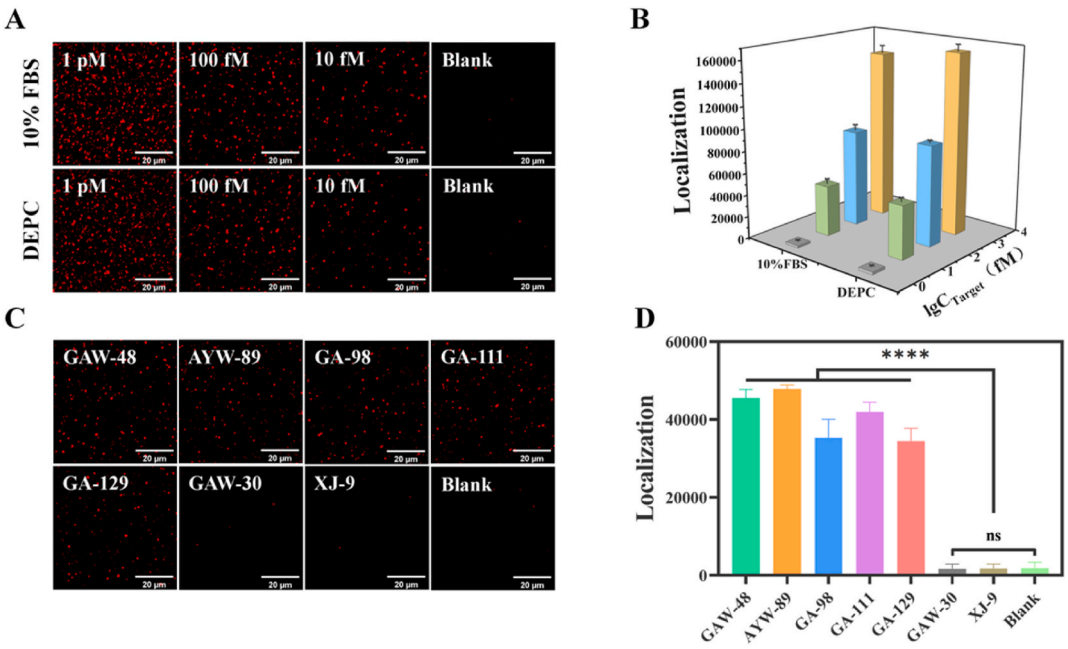


Fig. 4. The real sample detections of the DCP-platform. (A) The single-molecule fluorescence imaging of the magnetically separated supernatant with a series of concentrations (1 pM, 100 fM, 10 fM, and Blank) to the sample containing 10 % fetal bovine serum and DEPC-treated water. (B) The magnetically separated supernatant fluorescence localization counts. (C) The single-molecule imaging of magnetic separation supernatant after adding different RNA samples (GAW-48, AYW-89, GA-98, GA-111, GA-129, GAW-30, XJ-9, and Blank). (D) The counts fluorescence localization in real samples after magnetic separation supernatant imaging. $^{*}P < 0.05$, $^{**}P < 0.01$, $^{***}P < 0.001$, $^{****}P < 0.0001$, student's *t*-test. Error bars represent the standard deviation of three experiments.

accuracy and reliability. Compared to other CRISPR/Cas13a-based approaches [42,43], this platform requires no complex material synthesis or device fabrication, offering improved detection speed, sensitivity, and convenience (Table S2).

To evaluate the specificity of the proposed platform, we compared the fluorescence intensity and localization counts of the target RNA (HTNV-RNA) against non-complementary RNAs (sja-miR-2c-5p, BC, SARS-CoV-2, SARS-CoV and MERS-CoV) and their mixture (Mix). The results (Fig. 3E) demonstrated that the fluorescence signals from non-complementary RNAs exhibited negligible changes compared to the blank group. In contrast, only the groups containing the target RNA (HTNV-RNA and Mix) displayed a significantly enhanced fluorescence intensity. Similar trends were observed in single-molecule fluorescence imaging results (Fig. 3F–G and Movie S4), indicating that the developed sensing platform effectively distinguishes between target and non-target RNA while demonstrating good specificity.

3.5. Real sample testing

HTNV-RNA is typically present in the host's blood at low concentrations, making it a significant challenge to distinguish HTNV-RNA from substantial amounts of interfering substances. To evaluate the capacity of this platform for RNA detection in complex samples, we introduced target concentrations (1 pM, 100 fM, 10 fM and Blank) into samples containing 10 % fetal bovine serum (10 % FBS) or DEPC-treated water and performed detection using this platform. The results (Fig. 4A–B and Movie S5-6) revealed no statistically significant difference in the fluorescence localization signals at the same concentration between the two groups, demonstrating the stable RNA detection capabilities of this system in complex environments. Additionally, a spike-and-recovery experiment was conducted to validate the accuracy of the detection system. Various concentrations of HTNV-RNA (10 fM to 1 pM) were spiked into a sample containing 10 % fetal bovine serum as a simulated sample. As the concentration of HTNV-RNA decreased, the fluorescence localization counts exhibited a declining trend, with the

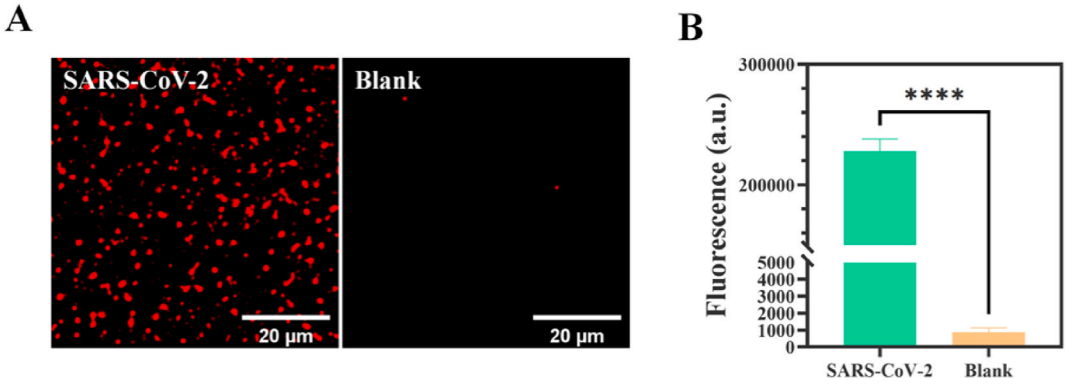


Fig. 5. The universal testing of the platform. (A) The schematic diagram of single-molecule fluorescence imaging of SARS-CoV-2 simulated samples. (B) The fluorescence localization analysis of single molecules after magnetic separation of SARS-CoV-2 simulated samples and 10 % fetal bovine serum (without target) samples. $^{*}P < 0.05$, $^{**}P < 0.01$, $^{***}P < 0.001$, $^{****}P < 0.0001$, student's *t*-test. Error bars represent the standard deviation of three experiments.

peak recovery rates ranging from 93.33 % to 111.43 % (Table 1). These results indicated that the sensing platform exhibited excellent accuracy and reliability.

Furthermore, nucleic acids were extracted from HTNV samples (GAW-48, AYW-89, GA-98, GA-111, GA-129) and Seoul virus (SEOV) samples (GAW-30, XJ-9) using a nucleic acid extraction kit and automatic nucleic acid extractor, followed by detection uing this platform. The results (Fig. 4C–D and Movie S7) revealed no significant Cy5 fluorescence signal in the two SEOV-infected samples, whereas all four HTNV-infected samples dispalyed markedly enhanced fluorescence signal. These findings demonstrated that the platform not only facilitated the detection of HTNV but also effectively distinguished SEOV, another viral species in the *Hantaviridae* family, showcasing remarkable sensitivity and specificity.

3.6. Versatility of the system

To verify the versatility of this system, we extended its application to SARS-CoV-2 RNA detection. Given that the sequence of the dumbbell-shaped hairpin is independent of the target RNA sequence, it can be utilized to detect any RNA by merely redesigning the hybridization region of the crRNA. The fluorescence spectra and single-molecule fluorescence localization imaging results (Fig. 5A–B, Fig. S9 and Movie S8) demonstrated that both the fluorescence signals and single-molecule fluorescence localization counts in the SARS-CoV-2 RNA group were significantly higher than those in the blank group. These results confirm the applicability of this platform for SARS-CoV-2 RNA detection, underscoring its broad utility. Moreover, these findings highlight the substantial potential of this sensing platform for future clinical molecular diagnostics.

4. Conclusion

In summary, we have developed a straightforward, rapid, sensitive, and specific diagnostic strategy based on CRISPR/Cas13a and DNA-PAINT, termed the DCP-platform, for the immediate detection of HTNV-RNA without the target amplification steps. This innovative platform employs a CRISPR/Cas13a reaction for target identification, combined with dumbbell-shaped hairpin cleavage-induced circular amplification and DNA-PAINT technology for signal amplification, achieving a remarkable triple signal enhancement. It offers a detection limit as low as the attomolar level, enabling accurate single-molecule RNA quantification. Our successful detection of HTNV in real samples, along with the differentiation of SEOV, underscores the method's exceptional sensitivity and specificity. The entire workflow can be completed in about 1 h, eliminating the need for pre-amplification, transcription, or centrifugation steps. This not only reduces detection time but also minimizes the potential for false positive results. Additionally, the sequence of hairpin-shaped structure is unrelated to the target sequence, enabling the diagnosis of various RNA types by simply redesigning the region of hybridization with crRNA. Our experimental results further demonstrated its capability to detect both Hantavirus RNA and Severe Acute Respiratory Syndrome Coronavirus 2 RNA (SARS-CoV-2 RNA). Consequently, this DCP-platform represents a 'five-in-one' RNA detection approach that integrates simplicity, versatility, accuracy, high specificity, and exceptional quantitative capability. However, this detection platform does have certain limitations. Currently, it is only capable of detecting RNA related to a single virus per test, which restricts its ability to meet the demand for simultaneous detection of multiple viral infections. This limitation hinders its application in diagnosing complex infectious diseases. To address these challenges, we plan to further optimize the platform by incorporating microfluidic technology in the future. Specifically, we aim to integrate the Cas13a cleavage reaction, magnetic separation, DNA-PAINT imaging, and other processes onto a single microfluidic chip. By leveraging the multi-channel capabilities of microfluidic chips and the programmability of crRNA, we intend to enable the synchronous detection of RNA related to multiple viruses. This innovative perspective on CRISPR/Cas13a-based RNA detection methods holds significant promise and broad application potential in clinical virus diagnostics.

CRediT authorship contribution statement

Jiamei Zhong: Writing – original draft, Methodology, Investigation, Data curation, Conceptualization. **Ziyue Xu:** Methodology, Formal analysis. **Jiawei Peng:** Investigation, Formal analysis, Data curation. **Liwen Guan:** Investigation, Formal analysis, Data curation. **Jianxiong Li:** Investigation, Data curation. **Zhuoxun Zhou:** Investigation, Data curation. **Yu Zhang:** Investigation, Data curation. **Jie Zhang:** Investigation, Data curation. **Shiwen Liu:** Writing – review & editing, Resources, Conceptualization. **Yifei Yang:** Writing – review & editing, Supervision, Project administration, Funding acquisition, Conceptualization. **Xian Hao:** Writing – review & editing, Supervision, Project administration, Funding acquisition, Conceptualization.

Declaration of competing interest

The authors declare that they have no known competing financial interests or personal relationships that could have appeared to influence the work reported in this paper.

Acknowledgments

This work was funded by the National Natural Science Foundation of China (No. 82160631 and 22277047), the Double Thousand Plan of Jiangxi Province (high-level talents project of scientific and technological innovation, No. 0210218606), Jiangxi Provincial Health Commission science and technology plan project (No. 202310087), the Development Grant of Jiangxi Provincial Key Laboratory of Epidemic Prevention and Control (No. 2024SSY06021), and Jiangxi Provincial Natural Science Foundation (20224BAB215040).

Appendix A. Supplementary data

Supplementary data to this article can be found online at https://doi.org/10.1016/j.talanta.2025.127852.

Data availability

Data will be made available on request.

References

[1] A. Jorgensen, I. Brandslund, C. Ellervik, T. Henriksen, A. Weimann, M.P. Andersen, C. Torp-Pedersen, P.K. Andersen, M.B. Jorgensen, H.E. Poulsen, Oxidative stress-induced damage to RNA and DNA and mortality in individuals with psychiatric illness, JAMA Psychiatry 81 (2024) 516–520, https://doi.org/10.1001/jamapsychiatry.2024.0052.

[2] M. Patchsung, K. Jantarug, A. Pattama, K. Aphicho, S. Suraritdechachai, P. Meesawat, K. Sappakhaw, N. Leelahakorn, T. Ruenkam, T. Wongsatit, N. Athipanyasilp, B. Eiamthong, B. Lakkanasirorat, T. Phoodokmai, N. Niljianskul, D. Pakotiprapha, S. Chanarat, A. Homchan, R. Tinikul, P. Kamutira, C. Uttamapinant, Clinical validation of a cas13-based assay for the detection of SARS-CoV-2 RNA, Nat. Biomed. Eng. 4 (2020) 1140–1149, https://doi.org/10.1038/s41551-020-00603-x.

[3] G. Yu, R. Chen, S. Zheng, Y. Liu, J. Zou, Z. Gu, B. Jiang, Q. Gao, L. Dai, J. Peng, J. Wang, F. Lu, A standardized assay for the quantitative detection of serum HBV RNA in chronic hepatitis B patients, Emerg. Microb. Infect. 11 (2022) 775–785, https://doi.org/10.1080/22221751.2022.2045874.

[4] Y. Yang, Z. Wang, H. Xie, Y. Hu, H. Liu, A SAW-based programmable controlled RNA detecting device: rapid in situ cytolysis-RNA capture-RNA release-PCR in one mini chamber, Adv. Sci. 11 (2024) e2309744, https://doi.org/10.1002/advs.202309744.

[5] J. Liu, L. Zhang, W. Zeng, L. Zhang, N. He, Z. Lu, High-throughput quantitative detection of triple-negative breast cancer-associated expressed miRNAs by rolling circle amplification on fluorescence-encoded microspheres, Chin. Chem. Lett. 34 (2023) 108141, https://doi.org/10.1016/j.cclet.2023.108141.

[6] C.B.F. Vogels, A.F. Brito, A.L. Wyllie, J.R. Fauver, I.M. Ott, C.C. Kalinich, M. E. Petrone, A. Casanovas-Massana, M. Catherine Muenker, A.J. Moore, J. Klein, P. Lu, A. Lu-Culligan, X. Jiang, D.J. Kim, E. Kudo, T. Mao, M. Moriyama, J.E. Oh, A. Park, N.D. Grubaugh, Analytical sensitivity and efficiency comparisons of SARS-CoV-2 RT-qPCR primer-probe sets, Nat. Microbiol. 5 (2020) 1299–1305, https://doi.org/10.1038/s41564-020-0761-6.

[7] Y. Fang, Y. Wang, L. Zhu, H. Liu, X. Su, Y. Liu, Z. Chen, H. Chen, N. He, A novel cartridge for nucleic acid extraction, amplification and detection of infectious disease pathogens with the help of magnetic nanoparticles, Chin. Chem. Lett. (2023) 108092, https://doi.org/10.1016/j.cclet.2022.108092, 1001-8417.

[8] J.S. Gootenberg, O.O. Abudayyeh, J.W. Lee, P. Essletzbichler, A.J. Dy, J. Joung, V. Verdine, N. Donghia, N.M. Daringer, C.A. Freije, C. Myhrvold, R. P. Bhattacharyya, J. Livny, A. Regev, E.V. Koonin, D.T. Hung, P.C. Sabeti, J. J. Collins, F. Zhang, Nucleic acid detection with CRISPR-cas13a/C2c2, Science 356 (2017) 438–442, https://doi.org/10.1126/science.aam9321.

[9] Y. Yang, F. Wang, B. Xue, X. Zhou, Field-deployable assay based on CRISPR-cas13a coupled with RT-RPA in one tube for the detection of SARS-CoV-2 in wastewater, J. Hazard Mater. 459 (2023) 132077, https://doi.org/10.1016/j.jhazmat.2023.132077.

[10] M. Zhang, H. Wang, H. Wang, F. Wang, Z. Li, CRISPR/Cas12a-Assisted ligation-initiated loop-mediated isothermal amplification (CAL-LAMP) for highly specific detection of microRNAs, Anal. Chem. 93 (2021) 7942–7948, https://doi.org/10.1021/acs.analchem.1c00686.

[11] A. Sen, M. Masetty, S. Weerakoon, C. Morris, J.S. Yadav, S. Apewokin, J. Tranguyen, M. Broom, A. Priye, Paper-based loop-mediated isothermal amplification and CRISPR integrated platform for on-site nucleic acid testing of pathogens, Biosens. Bioelectron. 257 (2024) 116292, https://doi.org/10.1016/j.bios.2024.116292.

[12] H. Lee, J. You, H. Lee, W. Kim, K. Jang, J. Park, S. Na, Enhanced selective discrimination of point-mutated viral RNA through false amplification regulatory direct insertion in rolling circle amplification, Biosens. Bioelectron. 252 (2024) 116145, https://doi.org/10.1016/j.bios.2024.116145.

[13] J. Zhang, Z. Chen, H. Lv, J. Liang, C. Yan, C. Song, L. Wang, Rapid and accurate SERS assay of disease-related nucleic acids based on isothermal cascade signal amplifications of CRISPR/Cas13a system and catalytic hairpin assembly, Biosens. Bioelectron. 253 (2024) 116196, https://doi.org/10.1016/j.bios.2024.116196.

[14] X. Gao, Y. Yin, J. Xie, S. Gong, X. Li, CRISPR/Cas13a-mediated triple signal amplification strategy for viral RNA detection, Sensor. Actuat. B- Chem. 422 (2025) 136706, https://doi.org/10.1016/j.snb.2024.136706.

[15] B. Shu, J.J. Yang, W.T. Chen, X. Li, Y.H. Xue, M.X. Liu, X.N. Yin, L. Xu, H.Z. Zhang, J.Y. Qiu, H.P. Zheng, Temperature-programmed microfluidic CRISPR diagnostics enable rapid and automatous point-of-care testing for syphilis, Chem. Eng. J. 154174 (2024) 1385–8947, https://doi.org/10.1016/j.cej.2024.154174.

[16] B. Luo, J. Zhou, X. Zhan, B. Ying, F. Lan, Y. Wu, Smartphone-based free-to-total prostate specific antigen ratio detection system using a colorimetric reaction integrated with proximity-induced bio-barcode and CRISPR/Cas12a assay, Small 20 (2024) e2310212, https://doi.org/10.1002/smll.202310212.

[17] Y. Yang, X. Li, X. Wang, Z. Wang, S. Gong, CRISPR-Cas-based colorimetric strategies for nucleic acids detection, TrAC-Trend. Anal. Chem. 182 (2025) 118058, https://doi.org/10.1016/j.trac.2024.118058.

[18] H. Zhang, M. Zhang, Y. Zhou, Z. Qiao, L. Gao, L. Cao, H. Yin, M. Wang, Organic photoelectrochemical transistor aptasensor for dual-mode detection of DEHP with CRISPR-cas13a assisted signal amplification, J. Hazard Mater. 470 (2024) 134175, https://doi.org/10.1016/j.jhazmat.2024.134175.

[19] W.W. Yang, M.L. Zhao, M.L. Liu, W.B. Liang, X. Zhong, Y. Zhuo, Circular DNAzyme-switched CRISPR/Cas12a assay for electrochemiluminescent response of demethylase activity, ACS Sens. 9 (2024) 344–350, https://doi.org/10.1021/acssensors.3c02025.

[20] H. Qian, X. Guo, H. Yang, T. Bao, Z. Wu, W. Wen, X. Zhang, S. Wang, Enhancing CRISPR/Cas-mediated electrochemical detection of nucleic acid using nanoparticle-labeled covalent organic frameworks reporters, Biosens. Bioelectron. 261 (2024) 116522, https://doi.org/10.1016/j.bios.2024.116522.

[21] L.W. Guan, J.W. Peng, T. Liu, S. Huang, Y. Yang, X. Wang, X. Hao, Ultrasensitive miRNA detection based on magnetic upconversion nanoparticle enhancement and CRISPR/Cas13a-Driven signal amplification, Anal. Chem. 95 (2023) 17708–17715, https://doi.org/10.1021/acs.analchem.3c03554.

[22] H. Chen, X. Ma, X. Zhang, G. Hu, Y. Deng, S. Li, Z. Chen, N. He, Y. Wu, Z. Jiang, Novel aerosol detection platform for SARS-CoV-2: based on specific magnetic nanoparticles adsorption sampling and digital droplet PCR detection, Chin. Chem. Lett. 34 (1) (2023) 107701, https://doi.org/10.1016/j.cclet.2022.07.044.

[23] Y.L. Ying, Z.L. Hu, S. Zhang, Y. Qing, A. Fragasso, G. Maglia, A. Meller, H. Bayley, C. Dekker, Y.T. Long, Nanopore-based technologies beyond DNA sequencing, Nat. Nanotechnol. 17 (2022) 1136–1146, https://doi.org/10.1038/s41565-022-01193-2.

[24] D. Nettels, A. Hoffmann, B. Schuler, Unfolded protein and peptide dynamics investigated with single-molecule FRET and correlation spectroscopy from picoseconds to seconds, J. Phys. Chem. B 112 (2008) 6137–6146, https://doi.org/10.1021/jp076971j.

[25] W.E. Moerner, M. Orrit, Illuminating single molecules in condensed matter, Science 283 (1999) 1670–1676, https://doi.org/10.1126/science.283.5408.1670.

[26] S. Dey, M. Dolci, P. Zijlstra, Single-molecule optical biosensing: recent advances and future challenges, ACS Phys. Chem. Au 3 (2023) 143–156, https://doi.org/10.1021/acsphyschemau.2c00061.

[27] L. Li, Y. Yu, C. Wang, Q. Han, X. Su, Transient hybridization directed nanoflare for single-molecule miRNA imaging, Anal. Chem. 91 (2019) 11122–11128, https://doi.org/10.1021/acs.analchem.9b01766.

[28] F. Ma, C.C. Li, C.Y. Zhang, Nucleic acid amplification-integrated single-molecule fluorescence imaging for in vitro and in vivo biosensing, Chem. Commun. 57 (2021) 13415–13428, https://doi.org/10.1039/d1cc04799j.

[29] R. Jungmann, C. Steinhauer, M. Scheible, A. Kuzyk, P. Tinnefeld, F.C. Simmel, Single-molecule kinetics and super-resolution microscopy by fluorescence imaging of transient binding on DNA origami, Nano Lett. 10 (2010) 4756–4761, https://doi.org/10.1021/nl103427w.

[30] J. Schnitzbauer, M.T. Strauss, T. Schlichthaerle, F. Schueder, R. Jungmann, Super-resolution microscopy with DNA-PAINT, Nat. Protoc. 12 (2017) 1198–1228, https://doi.org/10.1038/nprot.2017.024.

[31] J. Hellmeier, R. Platzer, A.S. Eklund, T. Schlichthaerle, A. Karner, V. Motsch, M. C. Schneider, E. Kurz, V. Bamieh, M. Brameshuber, J. Preiner, R. Jungmann, H. Stockinger, G.J. Schütz, J.B. Huppa, E. Sevcsik, DNA origami demonstrate the unique stimulatory power of single pMHCs as T cell antigens, Proc. Natl. Acad. Sci. U. S. A. 118 (2021) e2016857118, https://doi.org/10.1073/pnas.2016857118.

[32] T. Jet, G. Gines, Y. Rondelez, V. Taly, Advances in multiplexed techniques for the detection and quantification of microRNAs, Chem. Soc. Rev. 50 (2021) 4141–4161, https://doi.org/10.1039/d0cs00609b.

[33] R. Jungmann, M.S. Avendaño, M. Dai, J.B. Woehrstein, S.S. Agasti, Z. Feiger, A. Rodal, P. Yin, Quantitative super-resolution imaging with qPAINT, Nat. Methods 13 (2016) 439–442, https://doi.org/10.1038/nmeth.3804.

[34] C. Li, Y. Xie, X. Cheng, L. Xu, G. Yao, Q. Li, J. Shen, C. Fan, M. Li, Single-molecule assessment of DNA hybridization kinetics on dye-loaded DNA nanostructures, Small (2024) e2402870, https://doi.org/10.1002/smll.202402870.

[35] S. Kocabey, G. Chiarelli, G.P. Acuna, C. Ruegg, Ultrasensitive and multiplexed miRNA detection system with DNA-PAINT, Biosens. Bioelectron. 224 (2023) 115053, https://doi.org/10.1016/j.bios.2022.115053.

[36] Z.Y. Xu, L.W. Guan, J.W. Peng, S.Y. Huang, T. Liu, T. Xiong, Y.F. Yang, X.L. Wang, X. Hao, Ultra-sensitive and specificity quantitative detection of miRNA using a combined CRISPR/Cas13a and DNA-PAINT, Sensor. Actuat. B-chem. 395 (2023) 134451, https://doi.org/10.1016/j.snb.2023.134451.

[37] H. Ma, Y. Yang, T. Nie, R. Yan, Y. Si, J. Wei, M. Li, H. Liu, W. Ye, H. Zhang, L. Cheng, L. Zhang, X. Lv, L. Luo, Z. Xu, X. Zhang, Y. Lei, F. Zhang, Disparate macrophage responses are linked to infection outcome of Hantan virus in humans or rodents, Nat. Commun. 15 (2024) 438, https://doi.org/10.1038/s41467-024-44687-4.

[38] P. Guardado-Calvo, F.A. Rey, L.S. Handal, N.A. Kuzmina, L.M. Principe, S. A. Kwilas, R.K. Kim, N.S. Chapman, M.S. Porter, P. Guardado-Calvo, F.A. Rey, L. S. Handal, S.M. Diaz, I.A. Zagol-Ikapitte, M.H. Tran, W.H. McDonald, J. Meiler, J. X. Reidy, A. Trivette, A. Bukreyev, J.E. Crowe, Antigenic mapping and functional characterization of human new world Hantavirus neutralizing antibodies, Elife 12 (2023) e81743, https://doi.org/10.7554/eLife.81743.

[39] X.M. Hang, P.F. Liu, S. Tian, H.Y. Wang, K.R. Zhao, L. Wang, Rapid and sensitive detection of ebola RNA in an unamplified sample based on CRISPR-cas13a and DNA roller machine, Biosens. Bioelectron. 211 (2022) 114393, https://doi.org/10.1016/j.bios.2022.114393.

[40] J. Ding, X. Xu, Y. Deng, X. Zheng, T. Zhang, Comparison of RT-ddPCR and RT-qPCR platforms for SARS-CoV-2 detection: implications for future outbreaks of infectious diseases, Environ. Int. 183 (2024) 108438, https://doi.org/10.1016/j.envint.2024.108438.

[41] L. Kreitmann, L. Miglietta, K. Xu, K. Malpartida-Cardenas, G. D'Souza, M. Kaforou, K. Brengel-Pesce, L. Drazek, A. Holmes, J. Rodriguez-Manzano, Next-generation molecular diagnostics: leveraging digital technologies to enhance multiplexing in real-time PCR, Trends Anal. Chem. 160 (2023) 116963, https://doi.org/10.1016/j.trac.2023.116963.

[42] A. Seletsky, M.R. O'Connell, S.C. Knight, D. Burstein, J.H. Cate, R. Tjian, J. A. Doudna, Two distinct RNase activities of CRISPR-C2c2 enable guide-RNA processing and RNA detection, Nature 538 (2016) 270–273, https://doi.org/10.1038/nature19802.

[43] M. Xie, H. Liu, S. Wan, X. Lu, D. Hong, Y. Du, W. Yang, Z. Wei, S. Fang, C.L. Tao, D. Xu, B. Wang, S. Lu, X.J. Wu, W. Xu, M. Orrit, Y. Tian, Ultrasensitive detection of local acoustic vibrations at room temperature by plasmon-enhanced single-molecule fluorescence, Nat. Commun. 13 (2022) 3330, https://doi.org/10.1038/s41467-022-30955-8.